



Using magnetic levitation to produce cryogenic targets for inertial fusion energy: experiment and theory

Denis Chatain, Vadim Nikolayev

► To cite this version:

Denis Chatain, Vadim Nikolayev. Using magnetic levitation to produce cryogenic targets for inertial fusion energy: experiment and theory. *Cryogenics*, 2002, 42 (3–4), pp.253-261. 10.1016/S0011-2275(02)00024-3 . hal-01261377

HAL Id: hal-01261377

<https://hal.science/hal-01261377>

Submitted on 25 Jan 2016

HAL is a multi-disciplinary open access archive for the deposit and dissemination of scientific research documents, whether they are published or not. The documents may come from teaching and research institutions in France or abroad, or from public or private research centers.

L'archive ouverte pluridisciplinaire **HAL**, est destinée au dépôt et à la diffusion de documents scientifiques de niveau recherche, publiés ou non, émanant des établissements d'enseignement et de recherche français ou étrangers, des laboratoires publics ou privés.



Distributed under a Creative Commons Attribution - NonCommercial - NoDerivatives| 4.0 International License

Using magnetic levitation to produce cryogenic targets for inertial fusion energy: experiment and theory

D. Chatain and V. S. Nikolayev¹

*CEA/DSM/SBT/ESEME, CEA Grenoble, 17, rue des Martyrs, 38054, Grenoble
Cedex 9, France*

Abstract

We present experimental and theoretical studies of magnetic levitation of hydrogen gas bubble surrounded by liquid hydrogen confined in a semi-transparent spherical shell of 3 mm internal diameter. Such shells are used as targets for the Inertial Confinement Fusion (ICF), for which a homogeneous (within a few per-cent) layer of a hydrogen isotope should be deposited on the internal walls of the shells. The gravity does not allow the hydrogen layer thickness to be homogeneous. To compensate this gravity effect, we have used a non-homogeneous magnetic field created by a 10 T superconductive solenoid. Our experiments show that the magnetic levitation homogenizes the thickness of liquid hydrogen layer. However, the variation of the layer thickness is very difficult to measure experimentally. Our theoretical model allows the exact shape of the layer to be predicted. The model takes into account the surface tension, gravity, van der Waals, and magnetic forces. The numerical calculation shows that the homogeneity of the layer thickness is satisfactory for the ICF purposes.

Key words: ICF, IFE target, magnetic levitation

1 Introduction

Several concepts have been proposed for the design of a commercial power plant based on Inertial Fusion Energy production [1,2]. Targets are direct or indirect drive targets but must be at cryogenic temperature [3]. They must be injected in the vacuum chamber of the reactor at a rate of about 5 Hz and a speed depending on the temperature and the residual pressure of the vacuum vessel [4]. The targets are then tracked and hit on-the-fly with laser or heavy ion beams [5].

¹ Mailing address: ESEME-CEA, Institut de Chimie de la Matière Condensée de Bordeaux, CNRS, Avenue du Dr. Schweitzer, 33608 Pessac Cedex, France; e-mail: vnikolayev@cea.fr

The targets are hollow spherical shells made of beryllium or polystyrene. Their diameter ranges from 2 to 5 mm. Their internal wall must be covered with a solid layer of deuterium or a mixture of deuterium and tritium of several hundred microns in thickness. The thickness of the layer must be uniform within a few percent. If tritium is present in the mixture, the beta energy produced by tritium naturally drives the solid to a uniform thickness layer covering the internal walls of the shell [6,7]. If tritium is not present in the liquid layer, it stays at the bottom because of gravity. In this paper, we describe how, by using the diamagnetic properties of the hydrogen, we can compensate this gravity effect and obtain a homogenous thickness of liquid layer inside the sphere before freezing it.

2 Forces that act on hydrogen molecules

In order to obtain the homogeneous thickness of the liquid layer on the inner walls of a hollow spherical shell, one needs to satisfy simultaneously two conditions:

- the shape of the gas bubble inside the liquid should be spherical,
- the gas bubble should levitate in the middle of the shell.

We show now how the various forces influence the satisfaction of these conditions.

2.1 Surface tension

The force of the surface tension tends to minimize the interface area. Therefore, the surface tension helps to maintain the spherical shape of the gas bubble. Obviously, we need to look for the conditions where the value σ of the surface tension is large. As a matter of fact, σ is the decreasing function of the temperature T and goes to zero at the critical temperature T_c , which is about 33 K for hydrogen. The working temperature should thus be at least several degrees smaller than T_c .

The contribution of the surface tension (i.e. the Laplace pressure) is inversely proportional to the radius of curvature of the interface. For the thicker liquid layer the radius of the gas bubble is smaller and the Laplace pressure is thus larger. Therefore, the thickness of the thicker liquid layer is *a priori* more homogeneous (provided that the gas bubble is levitated in the middle of the shell) than the thickness of the thinner liquid layer. As a consequence, we need to analyze the homogeneity only for the thinnest layer under consideration, which is 200 μm . If for this case the homogeneity 1% criterion is satisfied, it will be satisfied for all larger thicknesses.

2.2 Van der Waals forces

Since the hydrogen completely wets the solid shell (zero contact angle), the van der Waals force manifests itself as an attraction between the hydrogen molecules and the solid wall [12]. It thus tends to create the layer of the densest (liquid) phase at the shell wall, leaving the less

dense phase (gas) in the middle of the shell. However, the value of this force is very small in comparison with the surface tension. While the van der Waals force influences strongly [12] the shape of the layers of microscopic (of the order of 1 μm) thickness, we do not expect a strong effect for the case of the thick liquid layers (average thickness larger than 200 μm), which we analyze in this report.

We carry out all our calculations for the non-retarded van der Waals interactions instead of the more suitable (because of the large layer thickness) retarded expression. The reason is that the retarded interactions are weaker [12] and would result in even smaller contribution.

2.3 Gravity and magnetic forces: magnetic levitation

The gravitational force per unit volume $f_g = \rho g$ is proportional to the mass density ρ of hydrogen, g being the gravitational acceleration. Since the liquid mass density ρ_L is larger than the gas mass density ρ_G , the resulting Archimedes force $\Delta\vec{f}_g = (\rho_G - \rho_L)\vec{g}$ that acts on the gas bubble tends to increase the thickness of the liquid layer on the bottom of the shell by lifting the bubble upwards. Gravitation thus needs to be compensated.

The gravity compensation by means of the static magnetic field is based on the expression for the magnetic force per unit volume $\vec{f}_m = \chi \nabla(B^2)/2\mu_0$ that acts on a body with the magnetic susceptibility χ , where B is the magnetic induction that would be created by the same solenoid in the free space and μ_0 is the magnetic permeability of free space. The magnetic susceptibility is proportional to the mass density ρ , $\chi/\rho = \alpha$ (see Table 1). The magnetic force that acts on

Table 1

Parameters of hydrogen at $T = 20$ K [11].

Description	Notation	Value	Units
Magnetic susceptibility/mass density	α	$-2.51 \cdot 10^{-8}$	m^3/kg
Surface tension	σ	0.002	N/m
Mass density of liquid phase	ρ_L	71.41	kg/m^3
Mass density of gas phase	ρ_G	1.19	kg/m^3

the bubble is thus (see Appendix)

$$\Delta\vec{f}_m = (\rho_G - \rho_L)\alpha \nabla(B^2)/2\mu_0 \quad (1)$$

and the condition of the bubble levitation is $\Delta\vec{f} = \Delta\vec{f}_m + \Delta\vec{f}_g = 0$.

Note that $\nabla(B^2)/2 = B_z dB_z/dz$ along the solenoid axis (axis z) and the curve $\Delta\vec{f}(z)$ exhibits a maximum (see Fig. 1) at some value of $z = z_m(I)$ that is almost independent of the solenoid current I .

All magnetic field calculations reported in this article were performed with the code BOBOZ translated to the C programming language. As an additional input to this code, the solenoid current in amperes multiplied by the number of coils is required.

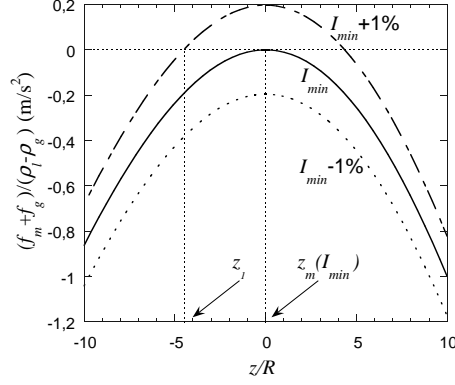


Fig. 1. The effective force per unit mass that acts on a small gas bubble in presence of the magnetic field of the solenoid versus z -coordinate along the solenoid axis calculated for three values of the solenoid current: I_{min} , $I_{min} \cdot 1.01$, and $I_{min} \cdot 0.99$.

Exact gravity compensation

$$g = \frac{|\alpha|}{\mu_0} B_z \frac{dB_z}{dz} \quad (2)$$

can be achieved when $I \geq I_{min}$, where I_{min} is a minimum current at which the exact compensation is possible at all. In the experiments (see sec. 3), the current I_{min} is 60 A. In our calculations we choose the point $z_m(I_{min})$ as a zero reference point. Its position is 8.502 cm above the solenoid center. According to our calculations, I_{min} corresponds to $1.8300 \cdot 10^6$ ampere-coils. The unknown (the solenoid documentation is not available) number of coils is obtained by division of this number by I_{min} .

Fig. 1 shows that when $I < I_{min}$, no compensation is possible at all, the force is non-zero everywhere. When $I > I_{min}$, there are two points of compensation z_1 and z_2 such as $z_1 < z_m < z_2$. However, it can be shown that levitation in z_2 is not stable, so that the compensation can be achieved in only one point $z_1 < z_m$. Everywhere else, the hydrogen molecules are exposed to the residual acceleration $\vec{\gamma} = |\alpha|/(2\mu_0) \nabla B^2 - \vec{g}$ the vertical (z) and radial (r) components of which are shown in Fig. 2. As we can see on these graphs, the radial component of the acceleration

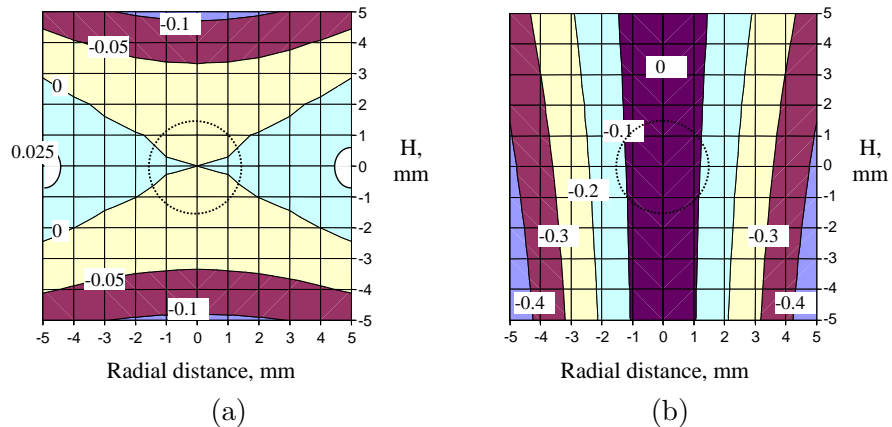


Fig. 2. The iso-acceleration curves for (a) γ_z and (b) γ_r . The position of the sphere is indicated by the dotted lines. The acceleration values are given in m s^{-2} .

in the vicinity of the center of the sphere is more important than the axial component. Inside

a 3 mm diameter sphere, the maximum radial acceleration is about 0.125 m s^{-2} , while the vertical acceleration is ten times lower. The radial acceleration is directed toward the vertical axis. This means that the interface can deviate from the spherical shape because it follows the variation of $\vec{\gamma}$. It is thus important to know if the homogeneous thickness of the liquid layer can in principle be achieved with the magnetic field created by the superconductive solenoid.

3 Experimental

3.1 Test facility

The test facility (Figs. 3) consists of a superconductive solenoid immersed into a helium bath. The vacuum vessel containing the sphere is introduced into the core of the solenoid. The sphere

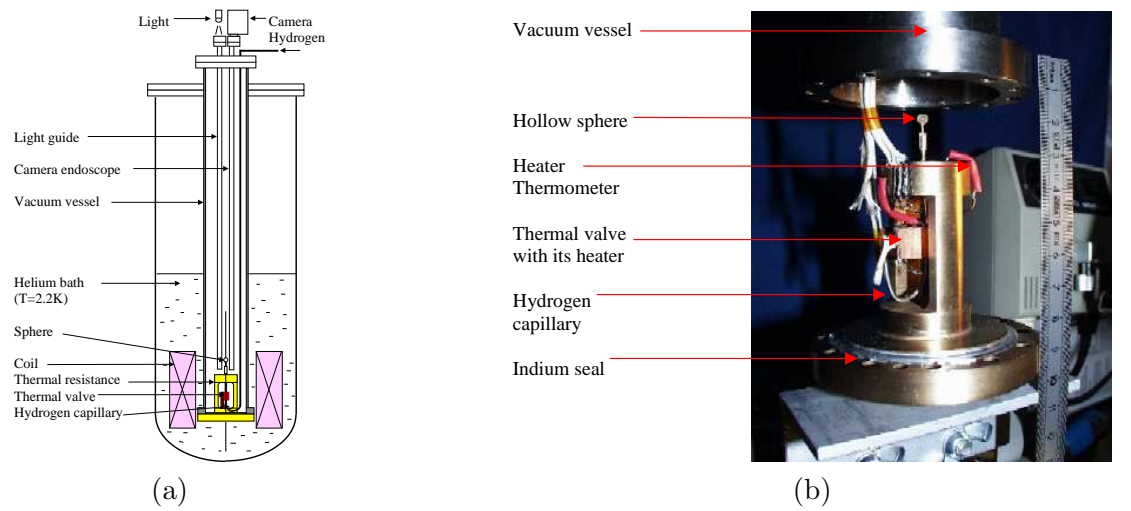


Fig. 3. (a) A scheme of the cryostat. (b) A photograph of the bottom of the cryostat showing the sphere.

is illuminated from the top of the cryostat with a light guide. Observation is performed with an endoscope and a CCD camera. The bottom of the cryostat with the sphere is shown in Fig. 3b. The sphere center is placed at 15 mm from the top of the solenoid i.e. into the calculated point $z_m(I_{min})$. The hydrogen is introduced into the sphere by capillary. The characteristics of the solenoid are listed in Table 2.

The following operations are performed in order to condense and levitate the hydrogen in the sphere:

- The vacuum vessel is pumped out to about 10^{-6} mb and the capillary is pumped out to about 0.1 mb.
- The solenoid and the vacuum vessel are cooled down to 2.2 K.
- The thermal valve is heated (a power of 300 mW is necessary)
- The sphere is heated to about 20 K.
- Hydrogen is slowly introduced into the capillary.

Table 2

Parameters of the superconductive solenoid.

Description	Value	Units
Inner radius	48	mm
Outer radius	93	mm
Total height	20	cm
B at 4.2 K and $I = 53$ A	8	T
B at 2.17 K and $I = 67$ A	10	T
Critical current at 2.17 K	72	A

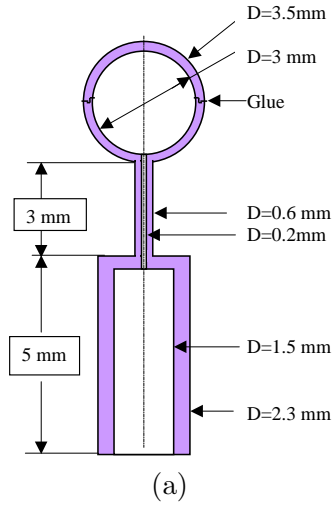


Fig. 4. (a) Design of the transparent hollow sphere. (b) A photograph of the sphere.

- When a sufficient quantity is condensed inside the sphere, the heater of the valve is cut so that an ice plug clogs up the capillary.
- The current in the solenoid is increased to about 60 A to compensate the gravity.
- The temperature of the sphere can be decreased below the triple point (13 K) to freeze the liquid.

3.2 Sphere

The sphere was made of Plexiglas (PMMA) machined in two hemispheres according to the design shown in Figs. 4. The two hemispheres were glued with *Epoxy 501* stick.

3.3 Effect of the magnetic field

As one can see in Figs. 5, it was possible to condense the hydrogen in the sphere. The optical imperfections of the sphere did not allow a high image quality to be obtained. Consequently, a precise measurement of the homogeneity of the layer thickness was not possible. Nevertheless,

we can see in Fig. 5d that the gas-liquid interface deformation due to the residual gravity force does not seem to be large.

The figures below show the effect of the magnetic field on the shape of the vapor bubble.

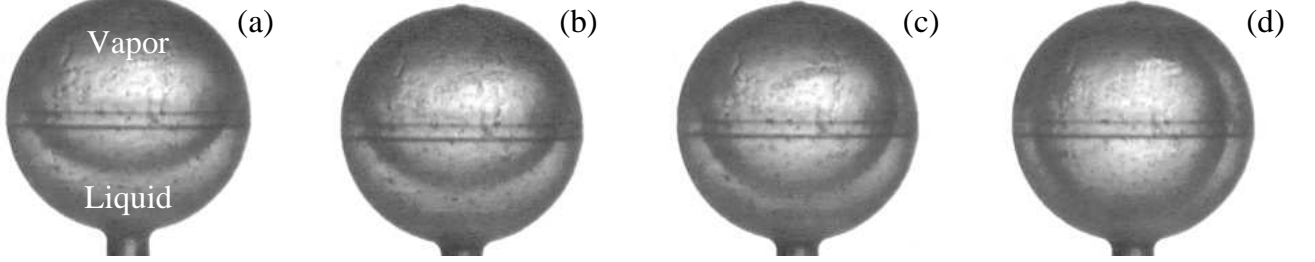


Fig. 5. The sphere half filled with liquid hydrogen at a temperature close to the triple point (14 K) for the different values of the current I in the solenoid that correspond to the different amplitudes of the magnetic field: (a) $I = 0$, (b) $I = 30$ A, (c) $I = 50$ A, (d) $I = 60$ A. The gravity is completely compensated by the magnetic force. The gas bubble is stable and well centered.

3.4 Effect of the liquid/vapor volume ratio

The images in Figs. 6 show the effect of the liquid/gas volume ratio for a gravity completely compensated by the magnetic field. This ratio controls the thickness of the liquid layer.

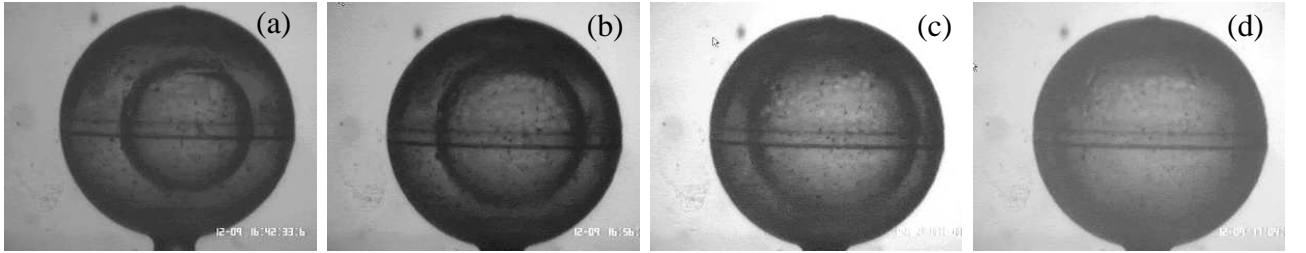


Fig. 6. Same as in Fig. 5d for the gravity compensation field and for the different liquid layer thickness: (a) $520 \mu\text{m}$, (b) $350 \mu\text{m}$, (c) $200 \mu\text{m}$, (d) It becomes difficult to measure the liquid layer thickness.

4 Numerical modeling

4.1 Mathematical formulation

The equilibrium shape of the interface can be found by two different approaches. One of them consists in direct numerical minimization of the free energy of the system. In this work we adopt another, variational approach, in which the minimization itself is performed analytically. It results in a variational equation that should be solved numerically to obtain the interface shape. The general form of this variational equation is the Laplace equation

$$K\sigma = \Delta p, \quad (3)$$

where K is the local curvature of the interface, and Δp is the difference between the forces per unit area that act on the interface from the liquid and gas sides. There are several contributions to Δp :

$$\Delta p = \Delta p_g + \Delta p_m + \Delta p_w + \lambda \quad (4)$$

that correspond to gravitation (Δp_g), magnetic field (Δp_m), and the van der Waals force (Δp_w). The constant λ is a Lagrange multiplier that appears as a result of the constrained gas volume V_G . λ can be viewed otherwise as an unknown *a priori* difference of pressures inside the liquid and gas phases.

The mathematical expression for the curvature K depends on the choice of the reference system and the independent variable. It is convenient to use the cylindrical (r, z) coordinate system because the solenoid (z) axis is vertical and $\Delta p = \Delta p(r, z)$ is thus cylindrically symmetric. In this reference system, the interface is fully defined by its half-contour for which $r > 0$.

None of the variables r, z can be chosen as independent because for the closed interface contour (at least) two values of z exists for each value of r and vice-versa. We choose as an independent variable the curvilinear coordinate l that varies along the interface contour counter-clockwise with $l = 0$ at the point on the symmetry axis where $r = 0$. Using this parameterization, $z = z(l)$ and $r = r(l)$. Since l measures the running length along the interface contour, the following equation is valid

$$z'^2 + r'^2 = 1, \quad (5)$$

where prime means the derivative d/dl . The expression for the local curvature then takes the form

$$K = r'z'' - r''z' + z'/r. \quad (6)$$

By introducing an auxiliary function $u(l)$, one can reduce (3) (with K given by (6)) to the set of the first-order ordinary differential equations:

$$\begin{cases} u' = \Delta p(r, z)/\sigma - \sin u/r \\ r' = \cos u \\ z' = \sin u \end{cases} \quad (7)$$

The physical meaning of the variable u can be found out by dividing two last equations: u is the angle between the r axis and the tangent to the interface contour.

The gas bubble volume V_G is fixed. This condition allows λ to be determined from the equation

$$V_G = \pi \int_0^L r^2 \sin u \, dl, \quad (8)$$

where $r = r(l)$ and $u = u(l)$ are the solutions of the set (7) and L is the unknown *a priori* half-length of the interface contour.

Four boundary conditions for the set (7) should be specified at the points $l = 0$ and $l = L$. Three of them serve to determine the integration constants in (7) and the fourth serves to determine L . There are two possible types of the boundary conditions. The first type corresponds to the case of the continuous liquid layer [12] and reflects the symmetry of the contour:

$$\begin{cases} u(0) = 0, \\ r(0) = 0, \\ u(L) = \pi, \\ r(L) = 0. \end{cases} \quad (9)$$

The boundary conditions of the second type should be specified when the liquid layer is discontinuous when the van der Waals forces are neglected in the calculation and the point $l = L$ is the triple (gas-liquid-wall) contact point. Since the contact angle is zero, the boundary conditions take the form

$$\begin{cases} u(0) = 0, \\ r(0) = 0, \\ r(L) = R \sin u(L), \\ z(L) = -R \cos u(L), \end{cases} \quad (10)$$

where R is the internal radius of the shell.

The mathematical problem is now complete. However, it is difficult to solve because of the moving boundary conditions specified at the unknown upper boundary L . This problem can be reduced to the simpler problem with the fixed boundary conditions by the following mathematical trick. We introduce new independent variable $\xi = l/L$ and two more dependent variables L and λ . The set (7) then reduces to

$$\begin{cases} u' = L \Delta p(r, z) - \sin u/r \\ r' = L \cos u \\ z' = L \sin u \\ L' = 0 \\ \lambda' = 0 \end{cases} \quad (11)$$

where u, r, z, L, λ are supposed to be the functions of ξ , prime means now the derivatives $d/d\xi$, and from now on we express r, z , and L in the units of R and Δp in the units σ/R . Five

unknown integration constants for these five equations should be found from the condition

$$V_G = \pi L \int_0^1 r^2 \sin u \, d\xi, \quad (12)$$

and from the four fixed boundary conditions (specified at $\xi = 0, 1$) for the problem of the first type (continuous liquid layer)

$$\begin{cases} u(0) = 0, \\ r(0) = 0, \\ u(1) = \pi, \\ r(1) = 0, \end{cases} \quad (13)$$

or of the second type (discontinuous liquid layer, i.e. direct wall-gas contact)

$$\begin{cases} u(0) = 0, \\ r(0) = 0, \\ r(1) = \sin u(1), \\ z(1) = -\cos u(1). \end{cases} \quad (14)$$

The set of equations (4,11,12) with the boundary conditions (13) or (14) provide two fully defined fixed boundary mathematical problems if the functional forms of $\Delta p_m(r, z)$, $\Delta p_g(r, z)$, and $\Delta p_w(r, z)$ are known. The magnetic induction B that enters the first of them (A.5) is calculated using the code BOBOZ. The second is given by $\Delta p_g(r, z) = \text{Bo} \cdot z$, where Bo is the non-dimensional Bond number

$$\text{Bo} = (\rho_L - \rho_V)gR^2/\sigma. \quad (15)$$

The expression for the van der Waals contribution was calculated in [12]. For the non-retarded interaction

$$\Delta p_w(r, z) = C_w [R_e^3(R_e^2 - d)^{-3} - (1 - d)^{-3}],$$

where $d = r^2 + z^2$, R_e is the external shell radius (1.75 mm) expressed in the units R and

$$C_w = \frac{4\pi}{3}(\rho_L - \rho_V) \frac{b_{HS} N_A^2 \rho_S}{\sigma R^2 m_S m_H} \quad (16)$$

is the non-dimensional number that reflects the strength of the van der Waals forces relative to the surface tension, $b_{HS} \approx 4 \cdot 10^{-78} \text{ J m}^6$ is the London constant for the interaction of the shell and hydrogen molecules, N_A is the Avogadro number, ρ_S and m_S is the mass density and the molecular weight of the shell material, and m_H is the molecular weight of hydrogen.

4.2 Calculation details

The mathematical problem (4), (11), (12), (14) with the boundary conditions of the second type was solved using the Shooting Method [15] for the two-point boundary value problems. This algorithm was modified slightly to include the condition (12) into the function *score* of [15]. The integral in (12) was calculated using the Simpson method. The set of the ordinary differential equations (11) was solved using the *rkdumb* function of [15] with 100 steps, which was sufficient to achieve the accuracy of 10^{-6} . The mathematical problem (4), (11), (12), (13) with the boundary conditions of the first type should be solved using the Shooting to the Fitting Point Method [15] because of the singularity $r = 0$ at the boundary point $\xi = 1$.

The calculations were performed for the values of the parameters shown in Table 2. The gas bubble volume V_G is defined by the average value for the liquid layer thickness of $200 \mu\text{m}$.

4.3 Levitation at minimum compensation current

The bubble shape calculated for the minimum compensation current I_{min} is presented in Figs. 7. Only right half of the interface Fig. 7a is calculated. The symmetric left half is added for illus-

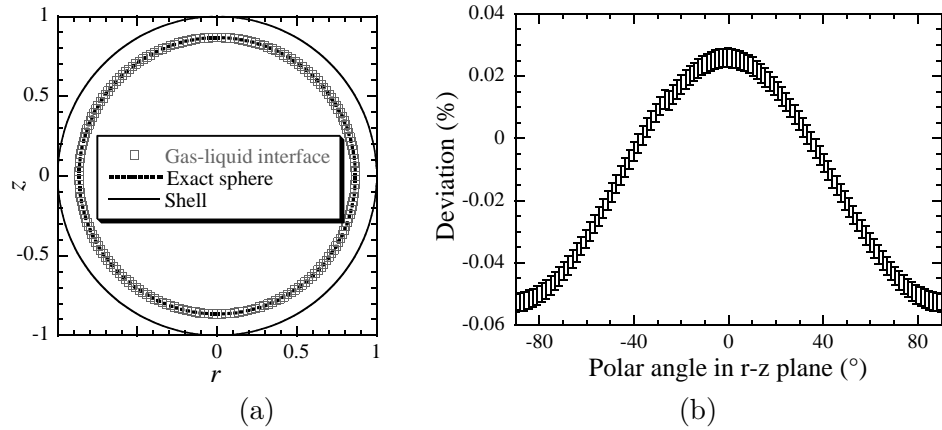


Fig. 7. (a) The shape of the gas-liquid interface at minimum compensation current I_{min} . All lengths are scaled by the cell inner radius $R = 1.5 \text{ mm}$. (b) Deviation of the shape in Fig. 7a from the spherical shape versus polar angle in the $r - z$ plane. Zero polar angle corresponds to the horizontal direction. The error bars show the numerical accuracy of the calculations.

tration purposes only to this and all other figures that show the interface shape. The interface resembles sphere very much, which explains the experimental result in Fig. 5d. However, there is a minor deviation from the sphericity, which is shown in Fig. 7b. In the case when the centers of the shell and of the interface coincide (it is easy to adjust experimentally by moving the shell with respect to the solenoid), this diagram gives the angular variation of the liquid layer thickness. Fig. 7b demonstrates that the liquid layer smoothness is at least one order better than 1% required for the ICF targets.

Because of the very small value of the van der Waals contribution (indeed, $C_w \sim 10^{-12}$), our code did not show any effect of the van der Waals forces within the numerical accuracy. The van der Waals forces should manifest themselves only when the gas bubble is pressed against the

shell. Due to them, a thin wetting layer (layer of liquid phase that separates the gas phase from the shell) forms even in this situation because of the complete wetting conditions. However, as the thickness of this layer is 100 to 1000 times less than the average thickness in our case, the chosen algorithm does not detect it and becomes unstable. Therefore, in the following we neglect the presence of the wetting layer, assuming that its thickness is zero, i.e. the liquid layer is assumed to be discontinuous, the boundary conditions of the second type (see section 4.1) being used for this case. We equally neglect the presence of the van der Waals forces for the case of the continuous liquid layer. The boundary conditions of the first type are applied in this case.

4.4 Levitated bubble: effect of the surface tension

In this subsection we consider the interface change under the influence of the decrease of the surface tension. Our experiments carried out for the temperatures close to the critical temperature of the hydrogen $T_c \approx 33$ K showed a wavy deformation of the gas-liquid interface. In this subsection we model the hydrogen bubble shape by neglecting the presence of the shell, i.e. by assuming the levitation of the gas bubble in the large volume of liquid. The results of the calculations are shown in Fig. 8. One can see that the bubble deformation increases when

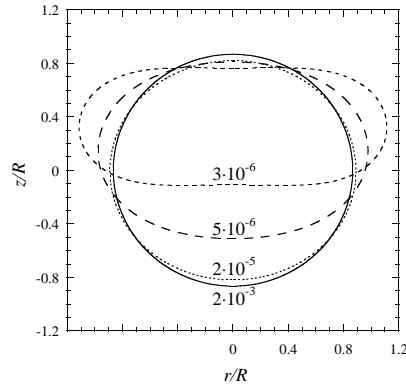


Fig. 8. The dependence of the shape of the gas bubble levitated in the infinite liquid on the surface tension σ , which is the parameter of the curves expressed in N/m. All shapes are calculated at minimum compensation current I_{min} . The bubble volume is fixed and corresponds to that of Fig. 7a.

the surface tension decreases to zero, the smallest value of the surface tension corresponding to the temperature of 30 mK below T_c . This deformation appears as a consequence of the residual acceleration $\vec{\gamma}$ inside the solenoid. Qualitatively, the deformation of the interface corresponds to the observations.

4.5 Levitated bubble: effect of solenoid current

The bubble shape calculated for the current one per cent larger than I_{min} is presented in Figs. 9. Comparing these figures with Figs. 7, two main differences become apparent. First, the equilibrium position of the bubble is displaced strongly to the bottom of the solenoid, its center corresponding approximately to the point z_1 from Fig. 1. In other words, the position of the

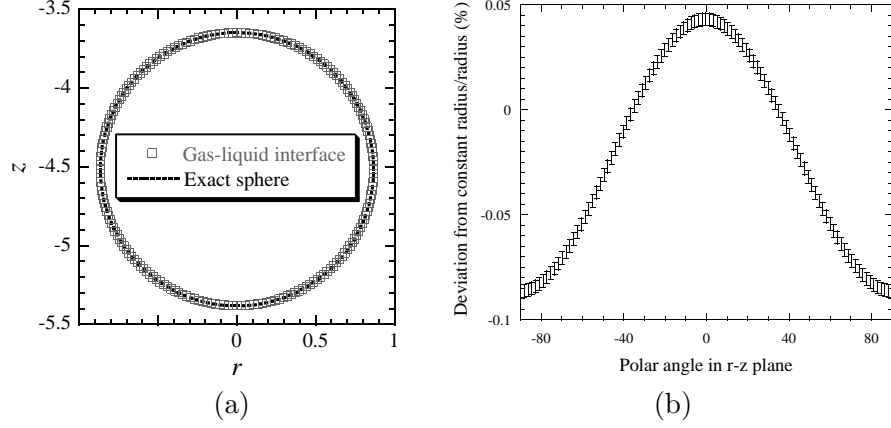


Fig. 9. (a) The shape of the gas bubble at the current value $I_{min} \cdot 1.01$. The other values of the parameters are the same as for Figs. 7. (b) Deviation of the shape in Fig. 9a from the spherical shape versus polar angle in the $r - z$ plane.

levitation point is very sensitive to the value of the current. Second, the maximum deviation from the average layer thickness is very sensitive to the current. Fig. 9b shows that the 1% increase of the current causes the $\sim 50\%$ increase in the maximum deviation.

For the current less than I_{min} , there is no equilibrium levitation position and the bubble is squeezed against the upper part of the shell.

4.6 Squeezed bubble

The squeezed bubble shapes calculated for current values smaller than $I_{min} = 60$ A are presented in Figs. 10. One can see that the variation of the current does not influence the shape strongly

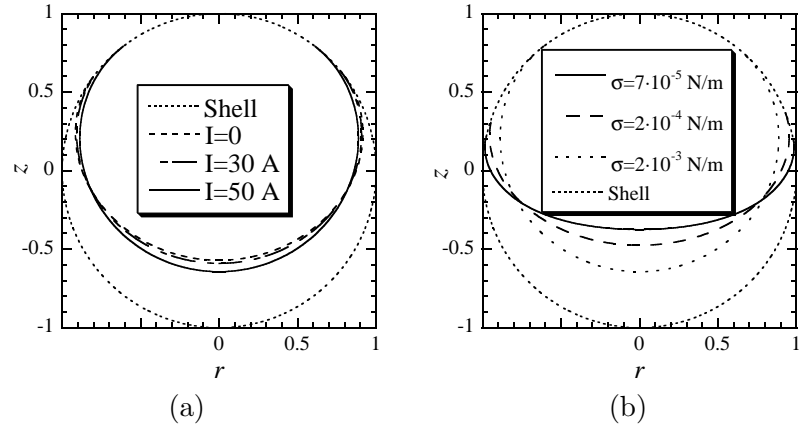


Fig. 10. The shapes of the gas bubble pressed against the shell calculated for: (a) different values of current and $\sigma = 0.002$ N/m; (b) different values of σ and current $I = 50$ A. The other values of the parameters are the same as for Figs. 7.

at a large value of the surface tension (Fig. 10a). These data compares well to the experiments. However, when the surface tension decreases, the inhomogeneity of the magnetic forces deform the bubble (Fig. 10b) in full analogy to the case of the levitated bubble shown in Fig. 8.

5 Conclusion and perspectives

The experiments of magnetic levitation of hydrogen, near the triple point, in a hollow semi-transparent spherical shell have been performed. Due to the fact that the sphere was not completely transparent, a precise characterization of the liquid layer could not be done. Nevertheless, the obtained images did not show deformation of the gas/liquid interface under the influence of the residual magnetic forces. Our numerical modeling of the gas-liquid interface shape shows that the layer of the liquid hydrogen with a very small thickness variation (less than 0.1%) can be achieved by means of magnetic levitation in a superconductive solenoid. The thickness homogeneity is the best when levitating at the minimum value of the current at which the levitation is possible at all. Although the levitation is possible at a higher value of the current, the thickness variation increases rapidly with the increase of the current. The higher homogeneity can be achieved for the a larger surface tension (smaller temperature) and a larger layer thickness provided that the gas bubble is well centered in the shell.

We investigate now the levitation in a coil based on the magnetic multipole concept. This coil is similar to coils used for the confinement of particles in accelerators. Such multipoles can levitate hydrogen or deuterium targets by tens or even hundreds at the same time. This could be a solution to the problem of high production rates required for commercial power plants based on the inertial fusion energy.

Acknowledgments

This work was supported in part by EURATOM. We thank Dr A. Dael of the laboratory of magnetism at CEA/Saclay and L. Quettier of the GREEN laboratory at Nancy for their advises on magnetostatics. We thank D. Beysens for the helpful discussions.

References

- [1] W.R. Meier, Osiris and Sombrero inertial power plant designs, *Fusion Eng. and Design* **25**, 145–157 (1994).
- [2] R.W. Moir et al., Hylife-II, a molten-salt inertial fusion energy power plant design, *Fusion Technol.* **25**, 5–25 (1994).
- [3] J T. Larsen, Why cryogenic inertial confinement fusion, *J. Vac. Sci. Technol.* **A7**, 1150–1156 (1989).
- [4] T. Norimatsu, A. Sunahara, K. Nagai, Influence of residual gas on the life of cryogenic target and trajectory of injected target, *Fusion Technology* **38**, 28 (2000).
- [5] R.W. Petzoldt and D. Goodin, Status of target injection and tracking studies for inertial fusion energy, *Fusion Technology* **38**, 22 (2000).
- [6] J.D. Simpson, J.K. Hoffer and L.R. Foreman, Beta-Layering of solid DT in a spherical polycarbonate shell, *Fusion Technology* **21**, 330–333 (1992).

- [7] A.J. Martin, R.J. Simms, and S.B. Wineberg, Beta heating driven DT ice redistribution, modeling studies, *J. Vac. Sci. Technol.* **A7**, 1157–1160 (1989).
- [8] E. Beaugnon, R. Tournier, Levitation of water and organic substances in high static magnetic field, *J. Phys. III (France)* **1**, 1423–1428 (1991).
- [9] M.V. Berry and K. Geim, Of flying frogs and levitrons, *Eur. J. Phys.* **18**, 307–313 (1997).
- [10] C.G. Paine, G.M. Seidel. Magnetic levitation of condensed Hydrogen, *Rev. Sci. Instrum.* **62**, 3022–3024 (1991).
- [11] C. Souers, *Hydrogen properties for fusion energy*, LLNL, University of California press, Berkeley and Los Angeles (1984).
- [12] L.S. Mok & K. Kim, *Phys. Fluids* **28**, 1227–1232 (1985).
- [13] M.A. Weilert, D.L. Whitaker, H.J. Maris & G.M. Seidel, *Phys. Rev. Lett.* **77**, 4840–4843 (1986).
- [14] L.D. Landau & E.M. Lifshitz, *Electrodynamics of continuous media*, Oxford (Pergamon), 2nd ed. (1963).
- [15] W.H. Press, S.A. Teukolsky, W.T. Vetterling & B.P. Flannery, *Numerical Recipes in C*, Cambridge University Press, 2nd ed. (1997).

A Appendix

Although the final expression for the magnetic contribution (A.4) can be found in the literature [13], we never met either its derivation or a discussion of the validity criterium. We address these two points in this appendix.

The absolute value for the normal component of the force per unit area p_m induced on an interface by the magnetic field (magnetic pressure) can be calculated in terms of the Cartesian components of the Maxwell tensor [14]

$$\sigma_{ik} = -\frac{1}{2}\mu\mu_0 H^2 \delta_{ik} + \mu\mu_0 H_i H_k, \quad (\text{A.1})$$

where $\mu = 1 + \chi$ is the magnetic permeability of the medium, H_i are the Cartesian components of the magnetic field, and δ_{ik} is the Kroneker symbol ($\delta_{ik} = 1$ if $i = k$ and 0 otherwise). The magnetic pressure is then

$$p_m = \sum_{i,k=1}^3 \sigma_{ik} n_i n_k = \frac{1}{2}\mu\mu_0 (H_n^2 - H_\tau^2), \quad (\text{A.2})$$

where n_i are the components of the external normal to the interface, H_n and H_τ are the normal and tangential components of the magnetic field, $H^2 = H_n^2 + H_\tau^2$. Using the boundary conditions

[14] for the magnetic field at the interface

$$\begin{cases} \mu_L H_{nL} = \mu_G H_{nG}, \\ H_{\tau L} = H_{\tau G}, \end{cases} \quad (\text{A.3})$$

where the indices L and G refer to the liquid and gas phases, one can obtain the expression

$$\begin{aligned} \Delta p_m = p_{mL} - p_{mG} &= -\frac{1}{2} \mu_0 (\mu_L - \mu_G) \left(H_{\tau G}^2 + \frac{\mu_G}{\mu_L} H_{nG}^2 \right) \approx \\ &= -\frac{1}{2} \mu_0 (\mu_L - \mu_G) H_G^2 \approx -\frac{1}{2\mu_0} (\mu_L - \mu_G) B^2, \end{aligned} \quad (\text{A.4})$$

where two approximations were used: $\mu_L \approx \mu_G \approx 1$. These approximate equalities verify with the accuracy 10^{-6} in our case and thus the final expression (A.4) can be employed.

The volume magnetic force (1) can be obtained from (A.4) using the integral Gauss theorem [14] as $\Delta \vec{f}_m = \nabla(\Delta p_m)$. By converting Δp_m into the a non-dimensional form, one obtains the final expression

$$\Delta p_m = \text{Mg} B(r, z)^2, \quad (\text{A.5})$$

where B is expressed in units of $B(0, 0)$, and

$$\text{Mg} = \frac{(\rho_L - \rho_G) |\alpha| R}{2\sigma\mu_0} B^2(0, 0) \quad (\text{A.6})$$

is the non-dimensional number that characterizes the strength of the magnetic force.